Electronic Supplementary Material (ESI) for ChemComm.

Phosphatase mechanism of bifunctional kinase/phosphatase AceK

Shu Wang[a], Qingya Shen[a], Guangju Chen[a], Jimin Zheng[a,*], Hongwei Tan[a,*] and Zongchao Jia[b,a]

[a] College of Chemistry, Beijing Normal University, Beijing, 100875 Beijing, CN; and [b] Department of Biomedical and Molecular Sciences, Queen's University, Kingston, Ontario, Canada K7L 3N6

[*] Correspondence should be addressed to jimin_z@bnu.edu.cn or hongwei.tan@bnu.edu.cn.

Supplementary Information

Supplementary Figure

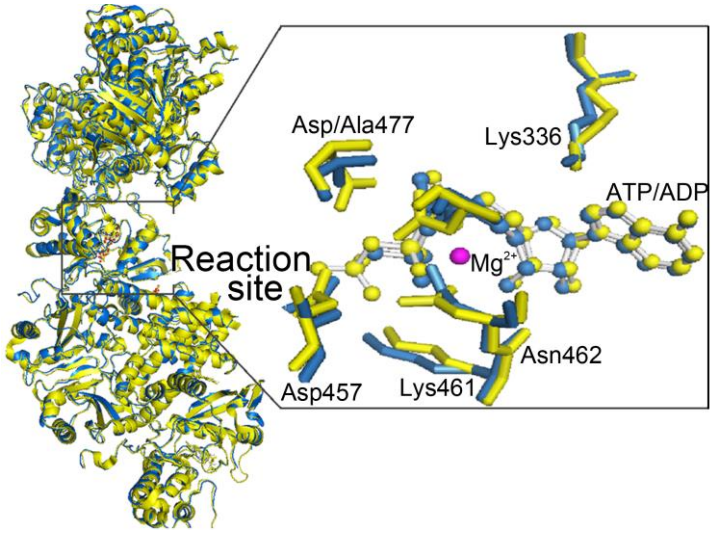

Fig. S1 Structural comparison of the AceK-IDH complex (PDB ID: 3LCB; yellow) and the AceK D477A-IDH complex (PDB ID: 4P69; blue). In D477A-IDH complex structure, no Mg^{2+} ion is found in active center. The reaction site are highlighted.

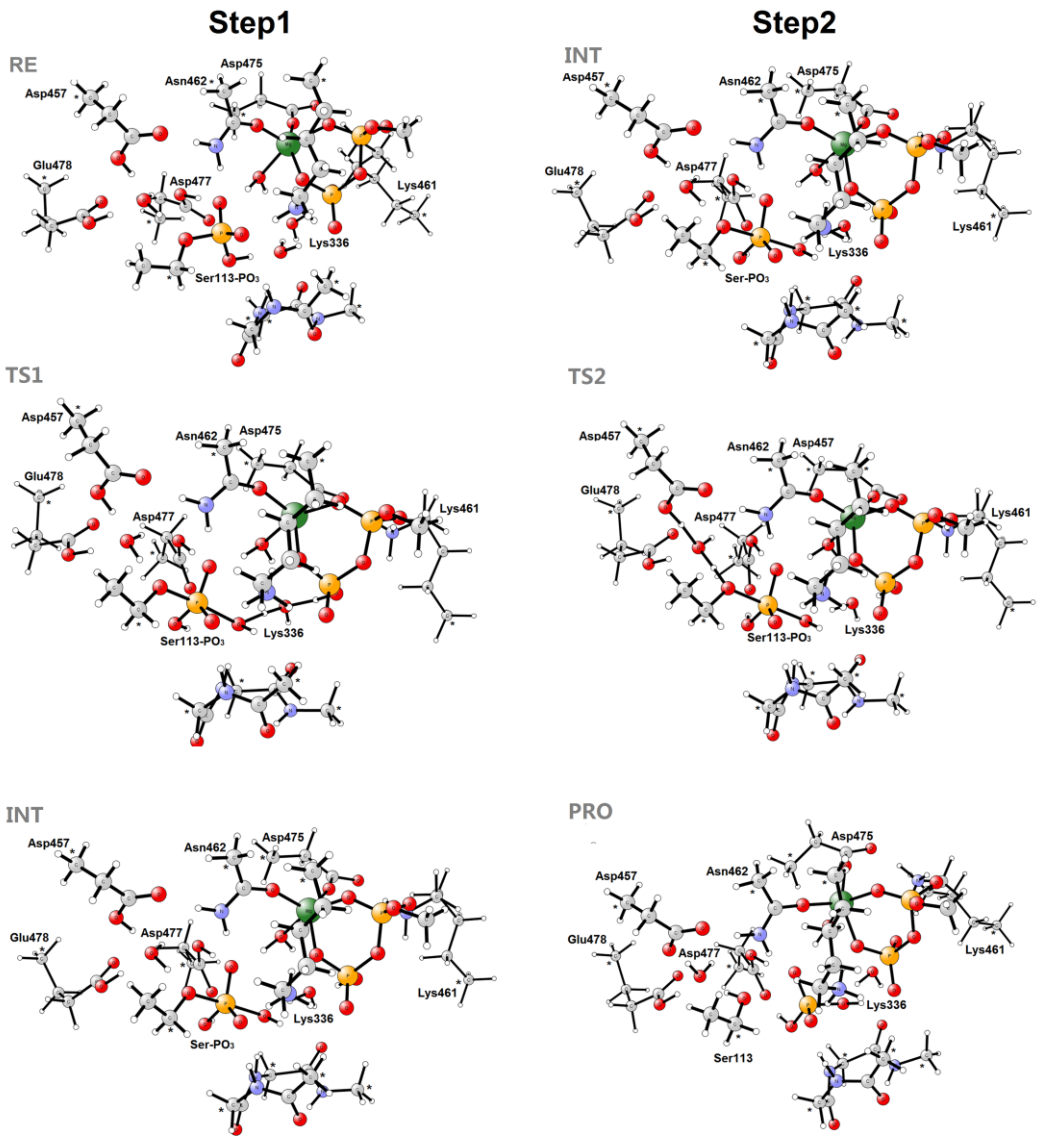

Fig. S2 Optimized structures of **RE**, **TS1**, **INT**, **TS2** and **PRO** for the two-step dephosphorylation process of AceK (PathwayI). Left column: critical structures located along the ADP proton accepter form a pentacoordinate phosphorus intermediate. Right column: critical structures located along the dephosphorylation reaction with proton transfer from Asp457.

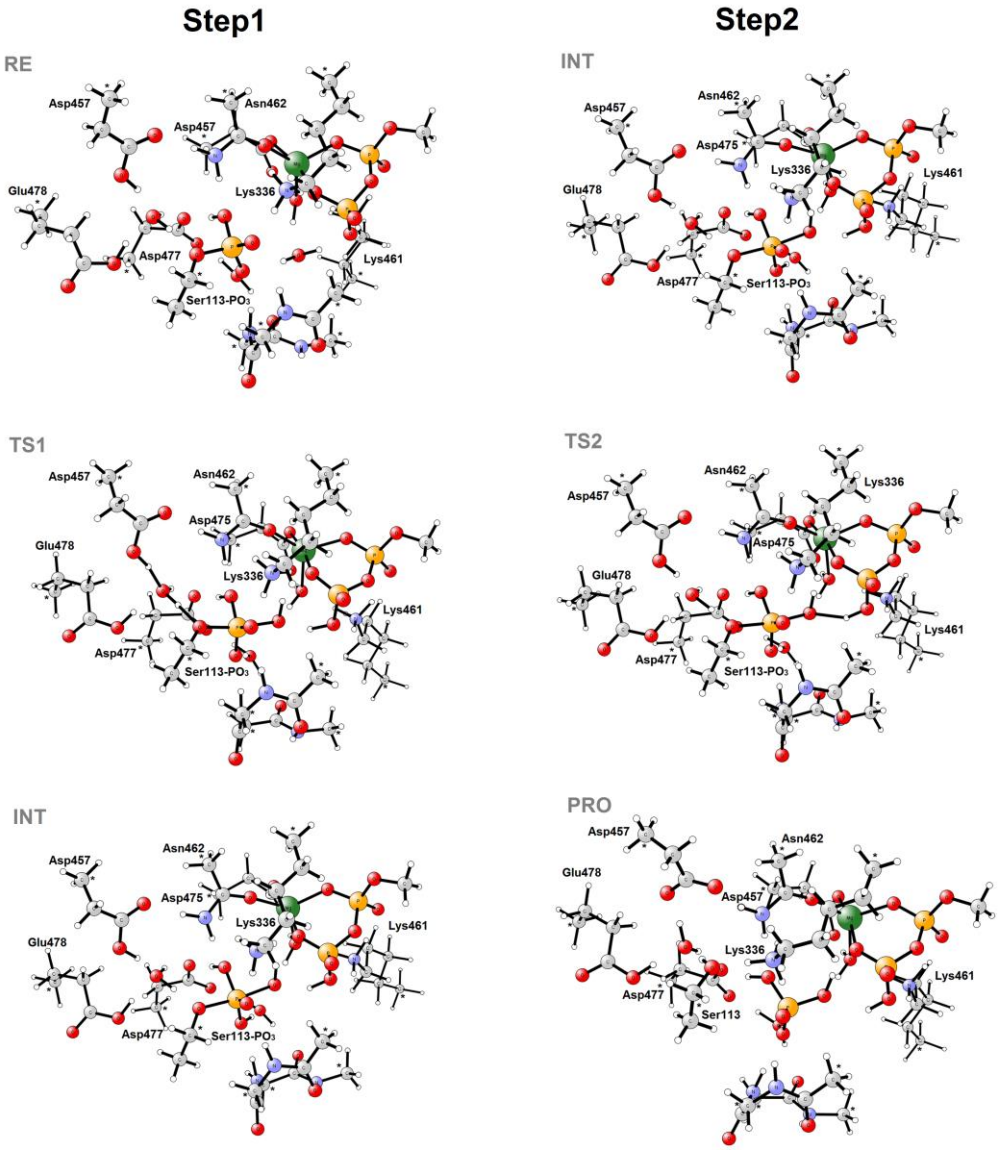

Fig. S3 Optimized structures of **RE**, **TS1**, **INT**, **TS2** and **PRO** for PathwayII. A water molecule interrupts one of the hydrogen bond between Asp477 and phosphoryl group in substrate. Left column: critical structures located along the ADP proton accepter form a pentacoordinate phosphorus intermediate. Right column: critical structures located along the dephosphorylation reaction with proton transfer from Asp457.

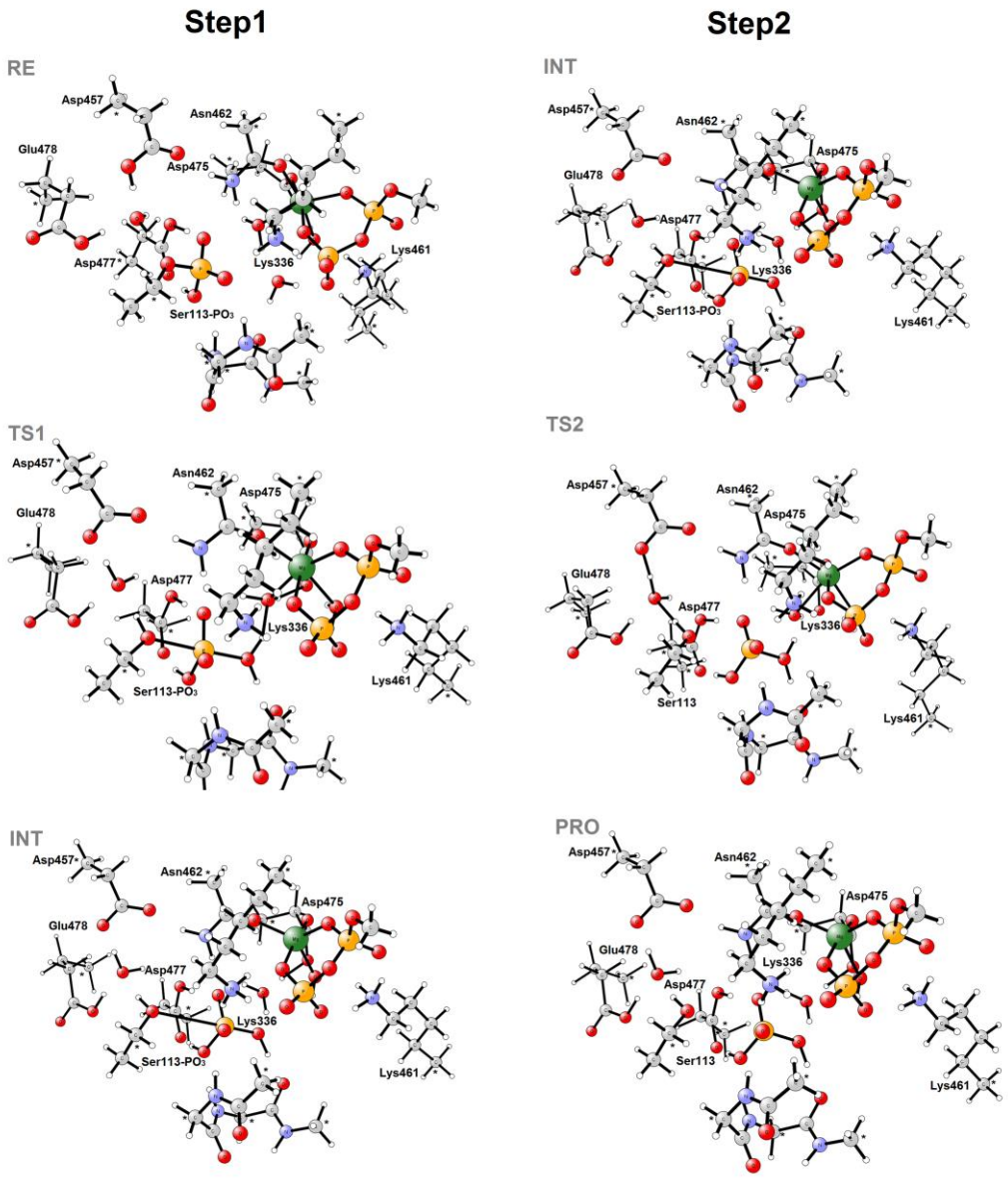

Fig. S4 Optimized structures of **RE**, **TS1**, **INT**, **TS2** and **PRO** for PathwayIII. Asp475 accept the proton from the water molecule. Left column: critical structures located along the Asp475 proton accepter form a pentacoordinate phosphorus intermediate. Right column: critical structures located along the dephosphorylation reaction with proton transfer from Asp457.

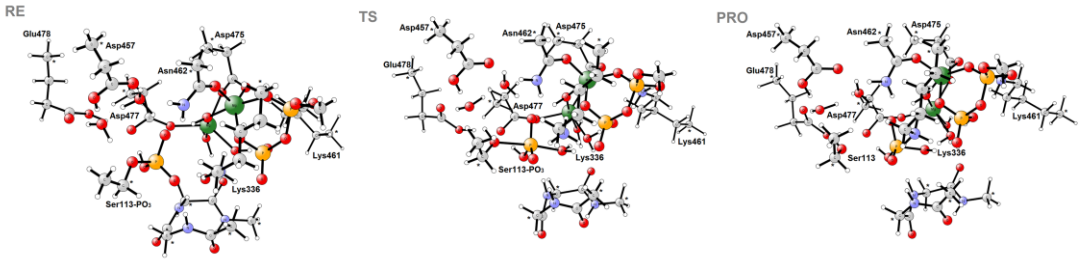

Fig. S5 Optimized structures of **RE**, **TS** and **PRO** for the PathwayIV. Double Mg^{2+} ions model indicates a stepwise pathway in dephosphorylation reaction with two Mg^{2+} ions. Critical structures are located along the two-step reaction.

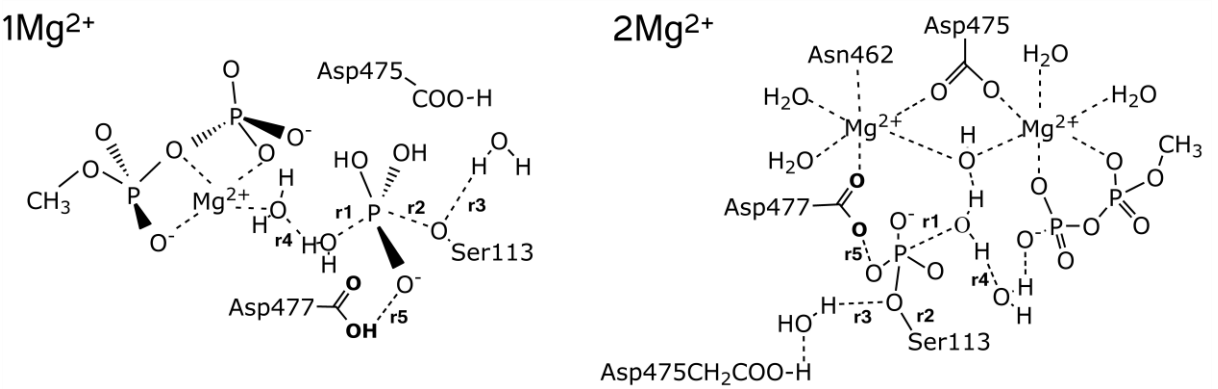

Fig. S6 Schematic diagram of $1Mg^{2+}$ and $2Mg^{2+}$ models. $1Mg^{2+}$ model contains only one Mg^{2+} ion, and corresponds specifically to PathwayI. $2Mg^{2+}$ model contains two Mg^{2+} ions, and corresponds to PathwayIV.

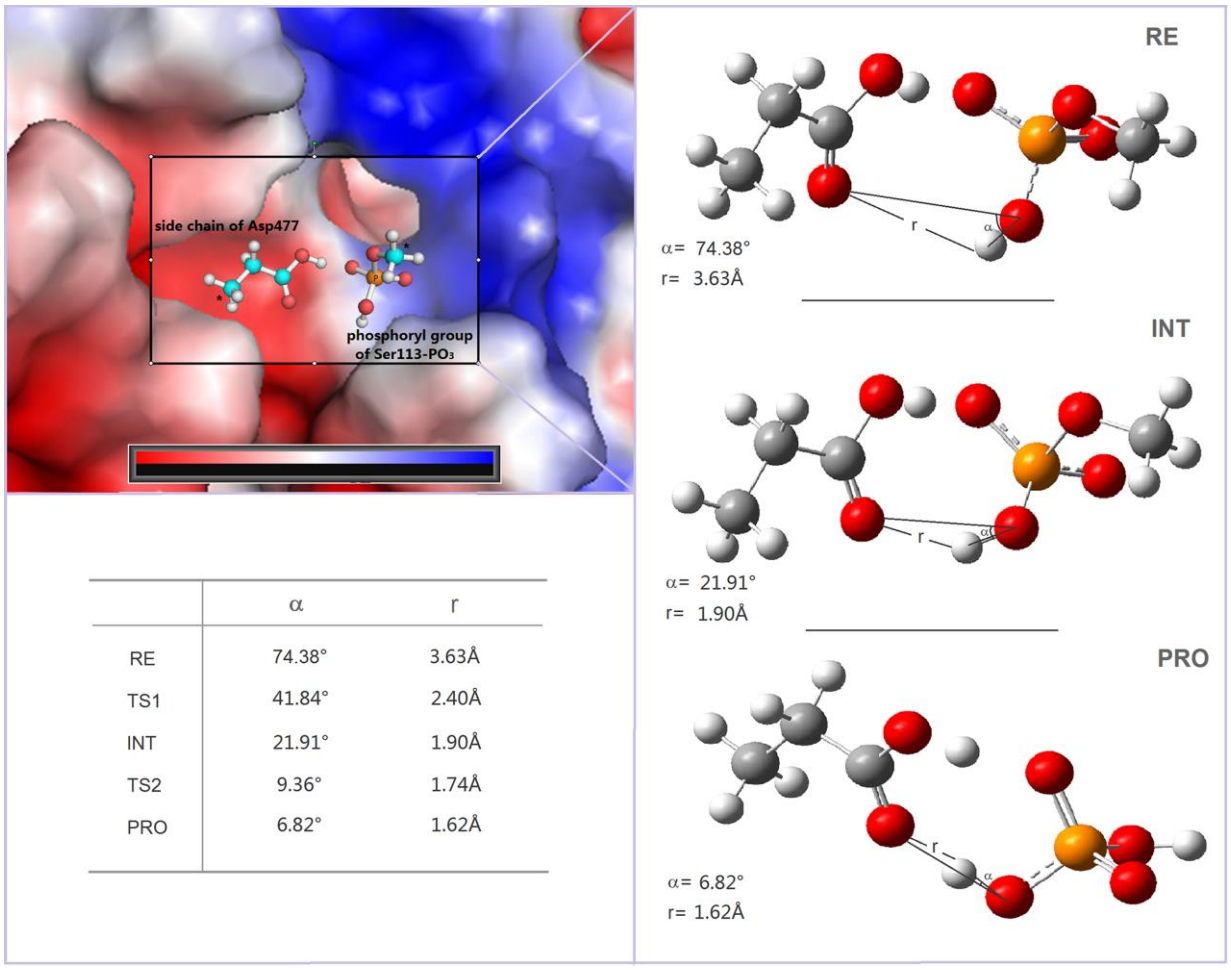

	α	r
RE	74.38°	3.63Å
TS1	41.84°	2.40Å
INT	21.91°	1.90Å
TS2	9.36°	1.74Å
PRO	6.82°	1.62Å

Fig. S7 Structural information regarding Asp477 and the phosphoryl group of Ser113-PO_3. Left column: the relative locations of Asp477 and Ser113-PO_3 in the AceK phosphatase conformation. Right column: structural information regarding Asp477 and the phosphoryl group of Ser113-PO_3 in reactant (**RE**), intermediate (**INT**) and product (**PRO**). Critical bond angles and lengths are also listed in the lower left area.

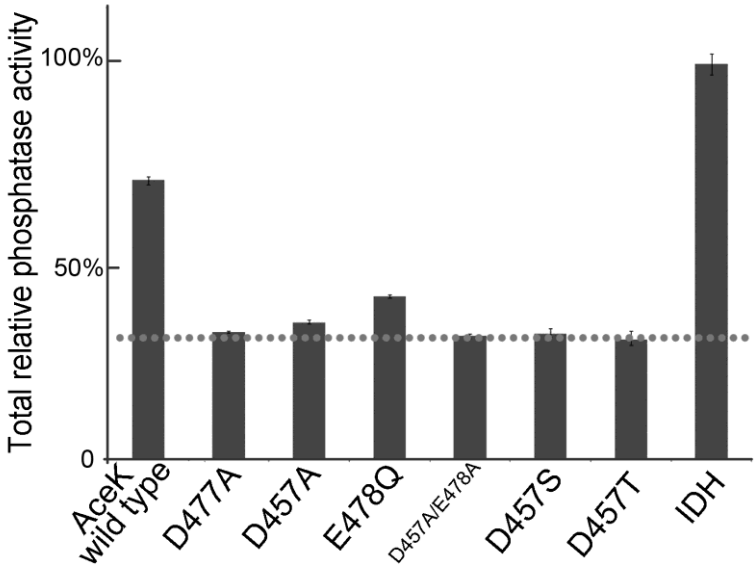

Fig. S8 Total relative phosphatase activity of AceK Asp457 and Glu478 mutants including background activity caused by residual IDH resulting from incomplete phosphorylation of IDH; error bars indicate the standard deviations.

Supplementary Table

Table S1. Statistics of X-ray diffraction data.

Protein form	**AceK D477A-IDH complex**
Wavelength (Å)	1.000
Space group	$P6_3$
Unit-cell parameters (Å)	a = b = 198.2, c = 156.1
Total number of reflections	379264
Number of unique reflections	27472 (4298)
Resolution (Å)	30-3.3
Completeness (%)	99.3 (98.6)
$\langle I/\sigma \rangle$	14.5 (2.7)
Redundancy	13.8 (8.6)
Molecules per AU	2
Rmerge (%)*	15.5 (85.6)
R/Rfree (%)	17.6/23.7
Solvent content	0.59

*$R_{merge} = \sum_{hkl}\sum_i|I_i(hkl)-\langle I(hkl)\rangle|/\sum_{hkl}\sum_i I_i(hkl)$, where $I_i(hkl)$ is the intensity of the i^{th} observation of reflection *hkl* and $\langle I(hkl)\rangle$ is the weighted average intensity of *i* observations of reflection *hkl*. Values in parentheses are for the highest resolution shell.

Table S2. Important distance (Å) for the various stationary points along the reaction pathways.[a]

	PathwayI					PathwayIV		
	RE	TS1	INT	TS2	PRO	RE	TS	PRO
r1	3.39	2.13	2.00	1.92	1.65	3.43	1.94	1.69
r2	1.65	1.74	1.77	1.87	3.20	1.66	2.18	3.22
r3	1.69	1.58	1.54	1.22	1.00	1.76	1.01	0.99
r4	1.54	1.05	1.03	1.02	1.00	1.71	1.58	1.03
r5	1.59	1.54	1.50	1.49	1.55	1.05	1.05	1.04

[a] see Fig. S6 $1Mg^{2+}$ and $2Mg^{2+}$

Supplementary Text

Details of methods

AceK D477A-IDH complex cloning, expression and purification. Hexahistidine-tagged IDH from *Escherichia coli* was over expressed in *E. coli* BL21(DE3) cells and purified using Ni^{2+}-NTA affinity resin (Qiagen) followed by size-exclusion chromatography.[1] The AceK D477A mutant was obtained by polymerase chain reaction using the forward primer 5'-GGGCGTGTGGTTTTTTATGATTACGCTGAAATTTGCTACAT- 3' and the reverse primer 5'-CACTTCCGTCATGTAGCAAATTTCAGCGTAATCATAAAAAA-3'. The resulting mutant protein was expressed in *E. coli* BL21 (DE3) cells. The purification of AceK D477A was similar to the procedure used for AceK.[1] The frozen IDH cells were suspended in 50 ml lysis buffer containing 50 mM Tris-HCl, pH 8.0, 300 mM NaCl. Cells were lysed on ice by sonication. Cell debris was removed by centrifugation for 30 min at 38,900 g using a R20A2 rotor in a HITACHI high-speed centrifuge. The clarified lysate was applied onto Ni^{2+}-NTA affinity resin (Qiagen) equilibrated with buffer A (30 mM Tris-HCl, pH 8.0, and 300 mM NaCl) followed by a ten-column-volume wash in lysis buffer containing 30 mM imidazole. The protein was eluted in several fractions by using a step gradient of increasing imidazole concentration up to 300 mM. The fractions were analyzed using 12.5% SDS-PAGE. The fractions containing protein were concentrated to 10 mg ml^{-1} using a Centricon-3 Merck Millipore and were further purified using an ÄKTA Purifier system (General Electric) with a size-exclusion HiLoad Superdex200 16/60 column in the buffer containing 20 mM HEPES, pH 7.0, 2 mM DTT, 100 mM NaCl and 10%(v/v) glycerol. The major protein peak was recovered and was concentrated to 8 mg ml^{-1} using a centrifugal filter unit (Amicon Ultra-15, 10 000, Merck Millipore). The purities of the AceK D477A and IDH proteins were estimated at ~95%.

AceK D477A-IDH complex crystallization. The purified IDH (46 kDa per subunit) and AceK D477A (68 kDa per subunit) were mixed in a 1:1 molar ratio in the presence of 1 mM ATP in a buffer consisting of 100 mM NaCl, 20 mM HEPES, pH 7.0, 2 mM DTT and 10%(v/v) glycerol. The mixture was stored at 277 K overnight, concentrated to 5-10 mg ml^{-1} (Merck Millipore) and purified further using an ÄKTA Purifier system (General Electric) with a size-exclusion HiLoad Superdex200 16/60 column in a buffer containing 25 mM HEPES, pH 7.5, 2 mM DTT, 100 mM NaCl and 10%(v/v) glycerol. The major protein peak was recovered and concentrated to 8 mg ml^{-1} (Amicon Ultra-15, Merck Millipore). The components of the peak were determined by SDS-PAGE. The preliminary crystallization conditions for the AceK D477A-IDH complex were screened by the sparse-matrix method[2] using standard screening kits. The protein was diluted to 5 mg ml^{-1} in the same protein buffer. ATP was added to a final concentration of 1 mM. The hanging-drop vapor-diffusion method was used. Hanging drops were set up to contain 2 µl protein solution mixed with 2 µl well solution and were equilibrated against 500 µl reservoir solution at room temperature. Crystals appeared in 3 days and grew to full size within two weeks. The optimal crystallization conditions in the reservoir were 10%(v/v) glycerol, 2 mM DTT, 50 mM magnesium chloride, 100 mM MES buffer, pH 6.0 with 25-30% PEG 300 as the precipitating agent at room temperature. A hexagonal crystal form was obtained.

AceK D477A-IDH complex X-ray data collection. Diffraction data were collected from the complex crystals at the NW12A beamline at the Photon Factory, KEK (High Energy Accelerator Research Organization, Tsukuba, Japan) using an ADSC Quantum 210 CCD detector at a wavelength of 1.000 Å. Prior to data collection, crystals were soaked in crystallization buffer containing 20%(v/v) glycerol for 1 min followed by flash-cooling using liquid nitrogen. The data set was collected at 100 K with an oscillation angle of 1.0 over a total of 180. The synchrotron data were indexed and integrated using *HKL*-2000[3]. The hexagonal crystal was determined to be of $P6_3$ symmetry and had unit-cell parameters a = b = 198.2 Å, c = 156.1 Å. A total of 379 264 reflections were collected in the resolution range 30-3.3 Å with an Rmerge of 0.155 and a completeness of 99.3%. Calculation of the Matthews coefficient suggested that each asymmetric unit (VM = 3.28 $Å^3$ Da^{-1}) contained two copies of the AceK D477A-IDH complex, corresponding to ~59% solvent content (Table S1).

Computational model and details. Calculation models were built using the high resolution (2.90 Å) structure of the AceK-IDH complex (PDB code: 3LCB). The phosphorylated substrate was represented by manual addition of a phosphoryl group to Ser113 in IDH. Furthermore, the buried Ser113 residue, with the phosphoryl group ~14.9 Å away from the Mg^{2+} ion in AceK active site, was repositioned in the AceK active site based on typical metal-dependent protein phosphatases PP2C (PDB code: 2CM1)[4], in which active-site residues were in the "near-attack" mode. This structure was subjected to energy minimization; 5,000 steps of minimization was carried out on side chains using the Amber 9.0 package with the Amber99 force field[5]. The charge parameters of ADP and AMP were determined by RESP (Restrained ElectroStatic Potential) fitting from the QM calculations. The cluster model was then built from the optimized complex structure, which contains the methyl-biphosphate arm of ADP, the Mg^{2+} ion and its coordinating residues, all of the first shell residues surrounding Ser113-PO_3 in IDH, including Asp457, Asp475, Asp477, Lys336, Lys461, Glu478 and Asn462 in AceK, and four important second-shell residues, Gly320, Met321, Val322 and Met323.

Asp475 and Asp477 were protonated to neutralize the condensed negative charges and three water molecules were added to coordinate with the Mg^{2+} ion to complete the coordination of Mg^{2+} ion. The resulting cluster model possesses a net charge of -1. Furthermore, in order to gain further mechanistic insights and information for comparison, an AceK model with two Mg^{2+} ions was also built and studied.

Based on the cluster model, the phosphatase mechanism was investigated by using the DFT functional B3LYP[6] with basis sets 6-31G(d,p) for P atoms and 6-31G for the rest. The energies reported herein were corrected for both solvation and zero-point vibrational effects[7] on the optimized structures. The polarization effects of the protein environment were estimated using the IEFPCM-UFF solvation model for core residues participating directly in the reaction (Ser113, Asp457, Asp477, Glu478, ADP and three water molecules). A dielectric constant of 4.0 with a probe radius of 1.4 Å solvent were used. Atomic radii of Mg^{2+} ion were corrected with the IDSCRF method to quantify more accurately the spatial extent of the molecular cavity.[8] Zero-point energy (ZPE) effects correction was performed at the same level as the geometry optimizations. All QM calculations were performed using the Gaussian03 program.[9]

Phosphatase activity assay. AceK mutants phosphatase activity was measured as follows.[10] For those mutants with uncompromised kinase activity, the AceK D477A mutant derivative, which retains kinase activity while lacking phosphatase activity, was used to produce Pi-IDH.[10] We first performed the IDH phosphorylation reaction using AceK D477A mutant by incubating the aforementioned phosphorylation reaction mixture for 1 h to ensure full phosphorylation of IDH. In a 96-well Falcon plate, 200 μl of phosphorylation reaction solution containing 20mM HEPES (pH 7.0), 1mM ATP, 2mM $MgCl_2$, 10mg IDH and 5 mg AceK D477A was incubated in each well for 1 h at 37 ℃. Next, we added to reaction solution the AceK mutants and a kinase inhibitor/phosphatase activator cocktail containing 5mM AMP and 5mM pyruvate, which inhibits AceK kinase activity and activates phosphatase activity. After incubation for 30 min at 37 ℃ to allow dephosphorylation of IDH and reactivation of IDH kinase activity, 20 μl of the phosphorylation reaction solution in each well was transferred to 180 μl of reduction solution consisting of 20mM HEPES (pH 7.0), 1mM threo-D,L-isocitrate, 0.5mM $NADP^+$ and 2mM $MgCl_2$. The activity of IDH was detected spectrophotometrically by monitoring the reduction of $NADP^+$ at 340nm using a PowerWave XS plate reader (Bio-Tek Instruments).[11] As a control, IDH alone was assayed for its activity of reducing $NADP^+$ using the same method. Because dephosphorylation of IDH by AceK removes inhibition of the activity of IDH, lower AceK phosphatase activity results in lower IDH activity. To test the feasibility of this new method, we first assayed IDH activity for IDH only (as a control) and for wild-type AceK, with and without the cocktail. In the presence of the cocktail, AceK exhibited clear phosphatase activity. In comparison, the cocktail did not affect IDH alone.[10] Phosphatase activity of AceK with different nucleotides was performed by comparing AceK phosphatase activity in the presence and absence of ADP, ATP or AMPPCP. We first performed the IDH phosphorylation reaction using AceK D477A mutant by incubating the aforementioned phosphorylation reaction mixture for 1 h to ensure full phosphorylation of IDH. Prior to the phosphatase activity assay, dialysis was carried out to remove any remaining nucleotides from the kinase reaction. We dialyze the mixture for 4 h to remove the nucleotides in the phosphorylation reaction. Then we added to reaction solution a kinase inhibitor/phosphatase activator cocktail containing 5mM AMP and 5mM pyruvate, which inhibits AceK kinase activity and activates phosphatase activity. And different nucleotides was also added to reaction solution to determine their respective effects on phosphatase activity. After incubation for 30 min at 37 ℃ to allow dephosphorylation of IDH and reactivation of IDH kinase activity, we performed AceK mutants phosphatase assay by similarly monitoring the reduction of $NADP^+$ to NADPH at 340 nm.

Site-directed mutagenesis was performed using the QuikChange site-directed mutagenesis kit (Stratagene) to create the following mutant derivatives: D457A, E478Q, D457A and E478A, D457S, D457T. The resultant derivatives expressed and purified as previously described and their phosphatase activities assayed.

Supplementary Results

Details of AceK dephosphorylation mechanism (PathwayI). In the first step the reactant overcomes 21.93 kcal mol^{-1} barrier (Fig. 2A), and then forms a pentacoordinate phosphorus intermediate. The energy of the metastable intermediate is 0.98 kcal mol^{-1} lower than the **TS1**. Compared with the **INT**, the energy of the **TS2** is 2.01 kcal mol^{-1} higher in the second step. The energy of stable product energy is 18.45 kcal mol^{-1} lower than the **TS2**. During the process the attacking water molecule (Wat1) delivers a proton to the β-phosphoryl group of ADP, and the proton of Asp457 transfers to the O_{Ser113} atom through a water molecule (Wat2).

In the reactant (Fig. S2, **RE**), O_{Wat1} (Fig. 1, Wat1) is 3.39 Å away from the P_{sub} in substrate, while the substrate interacts with another water molecule (Fig. 1, Wat2) through a short hydrogen bond (H_{Wat2}-O_{Ser113} = 1.69 Å). The oxygen atom of this water also forms two strong hydrogen bonds with carboxyl groups of Asp457 (O_{Wat2}-H_{Asp457}=1.55 Å) and Glu478 (O_{Wat2}-H_{Glu478}=1.63 Å). The other hydrogen bond forms between the side chain of the protonated Asp477 and O_{PO3} in substrate with the distance of 1.59 Å. Furthermore, the amino group of the Lys461 side chain interacts directly via hydrogen bond with two key moieties in the

active site: the β-phosphoryl group of ADP (1.62 Å) and the phosphoryl group in the substrate (1.64 Å). Such a tight hydrogen bond network in the active site ensures the relevant residues to form the near-attack conformation ready for the reaction. The Mg^{2+} ion in the active site is coordinated by Asn462, Asp475, α- and β-phosphoryl groups of ADP, and two water molecules. The relative orientation of the nucleophilic terminal phosphoryl group of ADP as well as the hydrogen bond contact between it and the phosphoryl group in substrate are also favorable for a nucleophilic displacement with the proton transfer from the activated water (Wat1) to the β-phosphoryl group of ADP.

In the transition state of the first step (Fig. S2, **TS1**), the distance of P_{sub} and O_{Wat1} dramatically decreases from 3.39 Å in reactant to 2.13 Å, while the P-O_{Ser113} distance elongates from 1.65 Å to 1.74 Å. The tetrahedron of phosphoryl group in substrate distorts slightly so that a water molecule (Wat1) could be pulled closer to the entering substrate phosphoryl group to form a pentacoordinate intermediate. Remarkably, in the transition state the proton is still attached to the O_{Wat3}. The bond between the transfer proton and the O_{Wat1} becomes weaker but not broken completely (1.03 Å in **RE**, 1.51 Å in **TS1**) (Fig. S2). However, the hydrogen bond length between H_{Asp457} and O_{Ser113} decreases from 1.69 Å in **RE** to 1.58 Å in **TS1**, which is important for the transfer of the proton in the second step. In the **TS1**, a new hydrogen bond forms between phosphoryl group in substrate and the side chain of Asp477. This hydrogen bond stabilizes the trigonal bipyramid configuration of phosphoryl group to assist the phosphoryl group leaving completely. Frequency calculation confirms that the transition vector at **TS1** ($\nu \approx 86 icm^{-1}$) has a contribution to the movement of the phosphoryl group in substrate. Energetically, **TS1** has a barrier of 21.93 kcal mol^{-1} compared with **RE**.

In the intermediate stage (Fig. S2, **INT**), the O_{Ser113}-P bond length is slightly longer compared with that in **TS1** (1.74 Å in **TS1** and 1.79 Å in **INT**), while the P-O_{Wat1} bond becomes stronger (2.13 Å in **TS1** and 1.96 Å in **INT**). The protons of the water molecules (Wat1 and Wat3) transfer more thoroughly in **INT** than that in **RE**. The β-phosphoryl group of ADP, which acts as a proton acceptor in the reaction, has already been protonated in **INT** by accepting the proton of attacking water molecule (Wat1). In the back side of the pentacoordinate phosphorus intermediate, the distance of O_{Ser113}-H_{Wat2} decreases from 1.58 Å in **TS1** to 1.46 Å in **INT**. The two hydrogen bonds between the O_{Wat2}-$O_{\delta Asp457}$ and O_{Wat2}-$O_{\delta Glu478}$ both shorten over 0.1 Å. The side chain of Asp477 forms two hydrogen bonds with the oxygen of phosphoryl group in substrate. In **INT**, both the hydrogen bonds are stronger than those in **TS1**. Especially owing to the fact that the proton of the phosphoryl group in substrate keep moving towards the carboxyl group of the Asp477, the hydrogen bond interaction is significantly enhanced. The hydrogen bond networks stabilize the pentacoordinate phosphorus intermediate in presence of only one Mg^{2+} ion in active center. The structure and charge distribution of the intermediate is more conducive to further reaction: the intermediate accepting a proton and then completely release the phosphoryl group.

The second reaction step (Fig. S2, step2) evolves through a transition state (Fig. S2, **TS2**) for the phosphoryl group and simultaneous protonation of the side chain of Ser113. The transition vector at **TS2** ($\nu = 463.20 icm^{-1}$) is almost contributed by the movement of the proton's transfer that accompanies with the inversion of the configuration of P_{sub} during the electrophilic substitution. Geometrically, the electrophilic O_{Ser113} interacts with the H_{Wat2} through a hydrogen bond (O_{Ser113}-H_{Wat2} = 1.22 Å). Other hydrogen bond interactions of this water molecule (Wat2) form with the carboxyl groups of Asp457 and Glu478, which are also enhanced. With the forming of these hydrogen bonds, the P-O_{Ser113} length becomes longer (1.79 Å in **INT** and 1.92 Å in **TS2**). The double hydrogen bond between Asp477 and phosphoryl group both strengthen at **TS2**. Interestingly, the proton on phosphoryl group is approaching to the oxygen of Asp477 side chain and the distance is notably decreases (1.90 Å in **INT** and 1.74 Å in **TS2**).

In the product obtained from the dephosphorylation reaction (Fig. S2, **PRO**), the phosphoryl group completely departs from Ser113. The optimized $O_{Ser113}\cdots P_{sub}$ distance of 3.20 Å suggests a complete O $_{Ser113}$-P_{sub} bond breakage. In addition, after passing **TS2**, the proton on Asp457 transfers to the hydroxyl group of the Ser113. The deprotonated Asp457 interacts closely with the O_{Wat2} through a short hydrogen bond with a distance of 1.40 Å, and the same water also involves in a strong hydrogen bond with Glu478. The detached phosphoryl group continues to interact with Lys461 in the product state; the distance of hydrogen in protonated amino group of Lys461 to the oxygen atom of the phosphoryl group is 1.57 Å, which is shorter than the values observed in the reactant and transition states. This indicates an increased strength of the interaction between Lys461 and the leaving phosphoryl group.

Asp477. In the reaction pathway, Asp477 forms three vital hydrogen bonds to stabilize the transition states and the strong hydrogen interactions last through the dephosphorylation process. The robust stabilization interaction between protonated Asp477 and the phosphoryl group in substrate is thus favorable for the reaction. Meanwhile Asp477 forms other hydrogen bonds which gradually become shorter during the stepwise reaction (Fig. S7). The orientation of hydrogen atom in the phosphoryl group in substrate experience drastic change, and its movement towards Asp477 makes the bond angle between the O_{Asp477}-O_{1PO3} and H-O_{1PO3} (Fig. S7, α angle) smaller, leading to the three atoms almost aligned in **PRO**. Eventually the side chain of Asp477 and

the oxygen atoms of phosphoryl group are almost located in a plane and form double hydrogen bonds that are nearly parallel. The simultaneous hydrogen bonding interactions maximize the effect of Asp477 on the phosphoryl group.

Other residues important for dephosphorylation

Both Asp457 and Glu478 are conserved residues in phosphatases. According to our calculation, these residues synergistically initiate the electrophilic attack through a water molecule in the second step by forming hydrogen bonds with the water molecule. However, in the proposed pathway of other phosphatases, it is Asp457, rather than Glu478, loses its proton. The distance between the O_{δ} in these residues and O_{Ser113} in the substrate (2.48 Å of Asp457, 2.60 Å of Glu478) is determinant of which residue is the proton donor. The experimental results also validated the theoretical conclusion that Asp457 is an irreplaceable proton donor, and the role of Glu478 is important but not indispensable. Thus, this further supports the second step of the stepwise mechanism.

Optimized structures potential energy profile PathwayII. In PathwayII, the reaction could also follow the stepwise mechanism (Table1, PathwayII). In the reactant of the pathway (Fig. S3), a water molecule interrupts one of the hydrogen bond between Asp477 and the phosphoryl group in substrate. The proton of the attacking water molecule transfers to ADP finally. Without one of the hydrogen bonds between Asp477 and the phosphoryl group in substrate, the structure of transition state becomes unstable, and the energy barrier dramatically increases to 41.10 kcal mol^{-1}.

Optimized structures potential energy profile PathwayIII. In PathwayIII, the reaction could also follow the stepwise mechanism (Table1, PathwayIII). In the reaction (Fig. S4), the proton of the attacking water molecule transfers to the other water molecule which coordinates with Mg^{2+} ion, meanwhile the dissociated water molecule passes the proton to the proton accepter Asp475 finally.

Details of AceK with double Mg^{2+} ions (PathwayIV). Three more water molecules were added to fulfill the octahedral coordination for the second Mg^{2+} ion to produce the general double metal ions model. In this model the added Mg^{2+} ion is coordinated by Asp 477, Asp457 and four water molecules. Asp457 and a deprotonated water molecule are coordinated with the double Mg^{2+} ions. The two oxygen atoms of deprotonated carboxyl group of Asp457 are coordinated with different Mg^{2+} ions, and the coordination mode of aspartic acid is more common in PPMs than that in other phosphatases.[12] The proton states of the residues remain unchanged, and the total charge of the model is 0. The detailed structure information is provided in Fig. S5.

The concerted form and breakage of bonds with the distances of 1.94 Å and 2.18 Å in transition state change the proton distribution: the proton of the bimetal activated water molecule transfers to ADP, meanwhile on the other side of the phosphoryl group in substrate, another water molecule supplies a proton to the O_{Ser113} to replace the leaving phosphoryl group. In this pathway, the Glu478, instead of Asp457 in PathwayI, donates the proton finally. As shown in Table S1, the P-O_{Ser113} bond (r1) is completely broken in the **TS** for the two-step mechanism (Asp457 acts as the acid in pathwayI), and partially broken for the concerted mechanism (Glu478 acts as the acid in pathwayIV). It shows that Asp457 serves as a better acid. The transition vector in **TS** (ν= 66.36icm^{-1}) has a large contribution to the movement of the transferred hydrogen atom that accompanies the inversion of the configuration of the phosphoryl group during the nucleophilic substitution.

Refrences

1 J. Zheng, A. X. Ji and Z. Jia, *Acta crystallographica. Section F, Structural biology and crystallization communications*, 2009, **65**, 1153-1156.

2 J. Jancarik, W. G. Scott, D. L. Milligan, D. E. Koshland, Jr. and S. H. Kim, *Journal of molecular biology*, 1991, **221**, 31-34.

3 Z. Otwinowski and W. Minor, *Methods in enzymology*, 1997, **276**, 307-326.

4 A. Wehenkel, M. Bellinzoni, F. Schaeffer, A. Villarino and P. M. Alzari, *Journal of molecular biology*, 2007, **374**, 890-898.

5 D.A. Case, T.A. Darden, T.E. Cheatham, III, C.L. Simmerling, J. Wang, R.E. Duke, R. Luo, K.M. Merz, D.A. Pearlman, M. Crowley, R.C. Walker, W. Zhang, B. Wang, S. Hayik, A. Roitberg, G. Seabra, K.F. Wong, F. Paesani, X. Wu, S. Brozell, V. Tsui, H. Gohlke, L. Yang, C. Tan, J. Mongan, V. Hornak, G. Cui, P. Beroza, D.H. Mathews, C. Schafmeister, W.S. Ross, and P.A. Kollman, AMBER 9, University of California, San Francisco, 2006.

6 (a) C. Lee, W. Yang and R. G. Parr, *PHYSICAL REVIEW B*, 1988, **37**, 785-789; (b) A. D. Becke, *The Journal of chemical physics*, 1993, **98**, 1372-1377; (c) *The Journal of chemical physics*, 1993, **98**, 5648-5652.

7 A. J. M. Ribeiro, M. J. Ramos and P. A. Fernandes, *J. Chem. Theory Comput.*, 2010, **6**, 2281-2292.

8 J. Y. Tao, W. H. Mu, G. A. Chass, T. H. Tang and D.C. Fang, *International Journal of Quantum Chemistry*, 2013, **113**. 975-984.

9 M. J. Frisch, G. W. Trucks, H. B. Schlegel, G. E. Scuseria, M. A. Robb, J. R. Cheeseman, J. A. Montgomery, Jr., T. Vreven, K. N. Kudin, J. C. Burant, J. M. Millam, S. S. Iyengar, J. Tomasi, V. Barone, B. Mennucci, M. Cossi, G.

Scalmani, N. Rega, G. A. Petersson, H. Nakatsuji, M. Hada, M. Ehara, K. Toyota, R. Fukuda, J. Hasegawa, M. Ishida, T. Nakajima, Y. Honda, O. Kitao, H. Nakai, M. Klene, X. Li, J. E. Knox, H. P. Hratchian, J. B. Cross, C. Adamo, J. Jaramillo, R. Gomperts, R. E. Stratmann, O. Yazyev, A. J. Austin, R. Cammi, C. Pomelli, J. W. Ochterski, P. Y. Ayala, K. Morokuma, G. A. Voth, P. Salvador, J. J. Dannenberg, V. G. Zakrzewski, S. Dapprich, A. D. Daniels, M. C. Strain, O. Farkas, D. K. Malick, A. D. Rabuck, K. Raghavachari, J. B. Foresman, J. V. Ortiz, Q. Cui, A. G. Baboul, S. Clifford, J. Cioslowski, B. B. Stefanov, G. Liu, A. Liashenko, P. Piskorz, I. Komaromi, R. L. Martin, D. J. Fox, T. Keith, M. A. Al-Laham, C. Y. Peng, A. Nanayakkara, M. Challacombe, P. M. W. Gill, B. Johnson, W. Chen, M. W. Wong, C. Gonzalez, and J. A. Pople, GAUSSIAN03 (Revision B.04), Gaussian Inc., Pittsburgh, PA, 2003.

10 J. Zheng and Z. Jia, *Nature*, 2010, **465**, 961-966.

11 C. S. Stueland, K. Gorden and D. C. LaPorte, *The Journal of biological chemistry*, 1988, **263**, 19475-19479.

12 G. Hou and Q. Cui, *Journal of the American Chemical Society*, 2013. **135**. 10457-10469.